

# Domain Adaptation via Rebalanced Sub-domain Alignment

Yiling Liu<sup>1</sup> Juncheng Dong<sup>2</sup> Ziyang Jiang<sup>3</sup> Ahmed Aloui<sup>2</sup> Keyu Li<sup>2</sup> Hunter Klein<sup>2</sup> Vahid Tarokh<sup>2</sup>  
David Carlson<sup>3,4</sup>

## Abstract

Unsupervised domain adaptation (UDA) is a technique used to transfer knowledge from a labeled source domain to a different but related unlabeled target domain. While many UDA methods have shown success in the past, they often assume that the source and target domains must have identical class label distributions, which can limit their effectiveness in real-world scenarios. To address this limitation, we propose a novel generalization bound that reweights source classification error by aligning source and target sub-domains. We prove that our proposed generalization bound is at least as strong as existing bounds under realistic assumptions, and we empirically show that it is much stronger on real-world data. We then propose an algorithm to minimize this novel generalization bound. We demonstrate by numerical experiments that this approach improves performance in shifted class distribution scenarios compared to state-of-the-art methods.

## 1. Introduction

Supervised deep learning has achieved unprecedented success in a wide range of real-world applications (Ganin & Lempitsky, 2015). However, obtaining labeled data, which is crucial for supervised learning algorithms, may be costly, labor-intensive, and/or time-consuming in certain applications, particularly in medical and biological domains (Lu et al., 2017; Li et al., 2020). To address this problem, unsupervised domain adaptation (UDA) has been proposed to make use of available labeled data (Farahani et al., 2021). The goal of UDA is to transfer knowledge from a labeled source domain to a different but related unlabeled target do-

main. Efficient UDA is challenging as models trained on the source domain may not perform well on the target domain due to discrepancies in the distributions of the two domains hereafter referred to as domain shift (Wang & Deng, 2018; Sankaranarayanan et al., 2018; Deng et al., 2019).

To address the challenge of domain shift, most domain adaptation research has focused on reducing the distributional gap between the source and target domains (Shen et al., 2018; Liu et al., 2016; Isola et al., 2017; Tzeng et al., 2015; 2017; 2020; Ganin & Lempitsky, 2015; Ganin et al., 2016; Peng et al., 2018). These methods are supported by statistical learning theory for transfer learning (Ben-David et al., 2006; 2010; Mansour et al., 2012; Redko et al., 2017; Li et al., 2018). They also have achieved high performance by learning representations that are both discriminative and domain-invariant (Ganin & Lempitsky, 2015). However, these methods are somewhat limited in the sense that they only focus on matching the marginal distribution between domains while ignoring label distributions (Deng et al., 2019). This limitation may be significant since class distribution shifts across domains are common phenomena in real-world applications (Jiang et al., 2020; Japkowicz & Stephen, 2002; Chawla, 2009; Tan et al., 2019).

In this paper, we present *Domain Adaptation via Rebalanced Sub-domain Alignment* (DARSA), a novel UDA algorithm that addresses the class distribution shifting. Motivated by theoretical analysis of sub-domain-based UDA methods, DARSA provides state-of-the-art (SOTA) performance in various tasks. Specifically, we attempt to reduce the reweighted classification error and the reweighted discrepancy between the sub-domains of the source task and that of the target task in order to improve classification performance under class distribution shifts. The reweighting is based on a simple intuition: *important sub-domains in the target domain need more attention* (see Section 4.2 for details). By reweighting the sub-domains, we can significantly alleviate the shifted class distribution problem. This is demonstrated by the superior performance of DARSA compared to those of existing SOTA methods (see Sections 6.2 and 6.3).

The benefits of introducing sub-domain alignment can be visualized in one-dimensional space, as shown in Figure 1(a). After splitting the distributions into corresponding sub-

<sup>1</sup>Program in Computational Biology and Bioinformatics, Duke University School of Medicine, Durham NC, USA <sup>2</sup>Department of Electrical and Computer Engineering, Duke University, Durham, NC, USA <sup>3</sup>Department of Civil and Environmental Engineering, Duke University, Durham, NC, USA <sup>4</sup>Department of Biostatistics and Bioinformatics, Duke University, Durham, NC, USA. Correspondence to: David Carlson <david.carlson@duke.edu>.

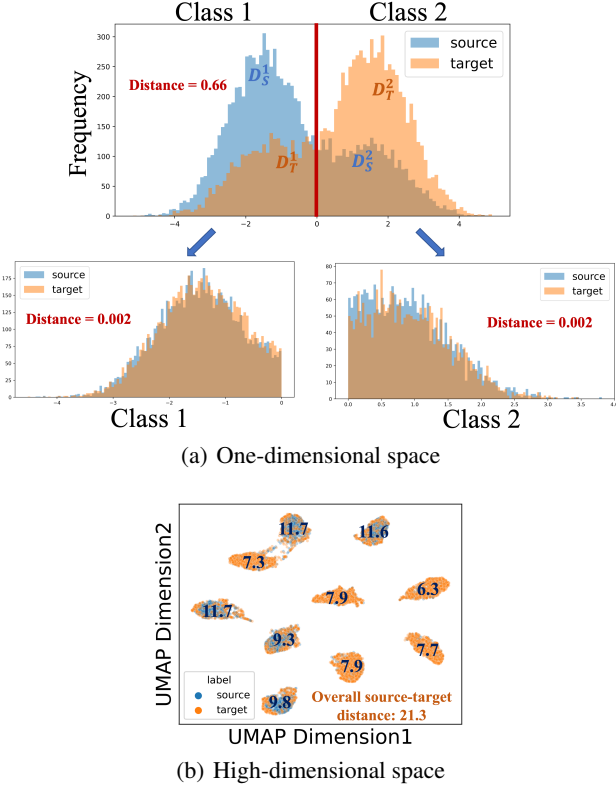


Figure 1. Illustration of the motivation. (a): The source domain (blue),  $\mathcal{D}_S$ , is sampled from a mixture of two Gaussians centered at  $-1.5$  and  $1.5$ , respectively with weights  $0.7$  and  $0.3$ . The target domain (orange),  $\mathcal{D}_T$  is sampled from a mixture of two Gaussian distributions centered at  $-1.4$  and  $1.6$ , respectively with weights  $0.3$  and  $0.7$ . The auxiliary variable  $\text{Class} \in 1, 2$  divides both domains into  $\mathcal{D}^1$  ( $x < 0$ ) and  $\mathcal{D}^2$  ( $x \geq 0$ ). (b) Distance between corresponding source-target sub-domains is shown for each cluster. Different clusters contain samples of different class labels. The distances are measured using Wasserstein-1 (W1) distance.

domains (e.g. sub-domains with the same label in the source and target task), we can focus on decreasing the distance between the corresponding source and target sub-domains. We also demonstrate the effectiveness of this method in high-dimensional and complex domain adaptation tasks through an experiment (see Section 6.2) where we transfer information from the MNIST (LeCun et al., 1998) dataset to the MNIST-M dataset (Ganin et al., 2016) under scenarios with shifted class distribution (e.g. different proportions of labels in the source and target domains). As illustrated in Figure 1(b), comparing with the distance between the source and target domains without aligning sub-domains, our method leads to a smaller distance.

We summarize our main contributions in this work below:

- We theoretically analyze UDA methods that align corresponding source-target sub-domains and establish a new generalization bound.

- We prove that our generalization bound is at least as strong as the state-of-the-art bounds for UDA problems with shifted class distribution under realistic assumptions. We also empirically demonstrate that our bound is much stronger on real-world datasets.
- Based on the proposed theory, we design an algorithm (DARSA) that reduces rebalanced distribution gaps between the source and target domains and rebalanced classification error by incorporating sub-domain structure.
- We demonstrate that DARSA outperforms state-of-the-art methods in shifted class distribution scenarios through experiments on both well-established benchmarks and real-world domain adaptation tasks.

## 2. Related Work

**Discrepancy-based Domain Adaptation.** A common goal of UDA is to reduce the distribution gap between the source and target domains. One approach to achieve this is discrepancy-based methods (Tzeng et al., 2014; Long et al., 2015; Sun et al., 2016), which often use maximum mean discrepancy (MMD) (Borgwardt et al., 2006) to directly match the marginal distributions of the source and that of the target domains. While MMD is a well-known Reproducing Kernel Hilbert Space (RKHS) metric, it is weaker than the Wasserstein-1 distance (Lu & Lu, 2020). Therefore, inspired by WDGR (Shen et al., 2018), our work uses the Wasserstein-1 distance as the distance metric. Many discrepancy-based methods also enforce the sharing of the first few layers of the networks between the source and target domains (HassanPour Zonoozi & Seydi, 2022). In contrast, our method lifts this restriction by allowing a more flexible feature space.

**Adversarial-based Domain Adaptation.** Adversarial-based domain adaptation methods aim to encourage domain similarity through adversarial learning (Shen et al., 2018; Liu et al., 2016; Isola et al., 2017; Tzeng et al., 2015; 2017; 2020; Ganin & Lempitsky, 2015; Ganin et al., 2016; Peng et al., 2018; Hoffman et al., 2018). These methods are divided into generative methods, which combine discriminative models with a generating process, and non-generative methods, which use a domain confusion loss to learn domain-invariant discriminative features (Wang & Deng, 2018). However, many existing algorithms fail to align multi-modal distributions under label shifting scenarios. Additionally, training adversarial networks can be challenging due to mode collapse and oscillations (Liang et al., 2018).

**Class-conditional Domain Adaptation.** Class-conditional domain adaptation has been used in a few existing methods to encourage alignment of multi-modal distributions and has shown improved performance in many tasks (Deng et al.,

2019; Shi & Sha, 2012; Jiang et al., 2020; Long et al., 2018; Snell et al., 2017; Pinheiro, 2018). In contrast to our work, none of these methods provides a theoretical perspective on the benefit of incorporating class-conditional structures.

**Theoretical Analysis of Domain Adaptation.** Many existing domain adaptation methods are inspired by generalization bounds based on the  $\mathcal{H}$ -divergence (Ben-David et al., 2006). The  $\mathcal{H}$ -divergence (Ben-David et al., 2006) is a modified version of the total variation distance ( $L_1$ ) that restricts the hypothesis to a given class. These generalization bounds can be estimated by learning a domain classifier with a finite Vapnik–Chervonenkis (VC) dimension. However, this results in a loose bound for most neural networks (Li et al., 2018). In our method, we use the Wasserstein distance for two reasons. First, the Wasserstein-1 distance is bounded above by the total variation distance employed by Ben-David et al. (2010). Additionally, the Wasserstein-1 distance is bounded above by the Kullback-Leibler divergence (a special case of the Rényi divergence when  $\alpha$  goes to 1 (Fournier & Guillin, 2015)), giving stronger bounds than those presented by Redko et al. (2017); Mansour et al. (2012). The second reason for leveraging the Wasserstein distance is that it has stable gradients even when the compared distributions are far from each other (Gulrajani et al., 2017).

### 3. Preliminaries

Given a labeled source domain  $X_S$  with distribution  $P_S$  and an unlabeled target domain  $X_T$  with distribution  $P_T$ , our goal is to learn a classifier that can accurately predict labels for the target domain using only the labeled source data and the unlabeled target data. Specifically, we have a labeled source dataset  $\{(x_S^i, y_S^i)\}_{i=1}^{N_S}$  and an unlabeled target dataset  $\{x_T^i\}_{i=1}^{N_T}$ . The source dataset has  $N_S$  labeled samples, and the target dataset has  $N_T$  unlabeled samples. We assume that the samples  $x_S^i \in \mathcal{X} \subseteq \mathbb{R}^d$  and  $x_T^i \in \mathcal{X} \subseteq \mathbb{R}^d$  are independently and identically drawn from the probability densities  $P_S$  and  $P_T$ , respectively. For mathematical rigor, we further assume that  $P_S$  and  $P_T$  are probability densities of Borel probability measures in Wasserstein space  $\mathcal{P}_1(\mathbb{R}^d)$ , which is the space of probability measures with finite first moment. Our goal is to learn a classifier  $f(x)$  that can accurately predict the labels  $y_T^i$ , given only the labeled source dataset  $\{(x_S^i, y_S^i)\}_{i=1}^{N_S}$  and the unlabeled target dataset  $\{x_T^i\}_{i=1}^{N_T}$ .

- *Sub-domain-related notations:* We assume that both  $X_S$  and  $X_T$  are mixtures of  $K$  sub-domains. In other words, we have  $P_S = \sum_{k=1}^K w_S^k P_S^k$  and  $P_T = \sum_{k=1}^K w_T^k P_T^k$  where we use  $P_S^k$  and  $P_T^k$  to represent the distribution of the  $k$ -th subdomain of the source domain and that of the target domain respectively. Note

that  $\mathbf{w}_S \doteq [w_S^1, \dots, w_S^K]$  and  $\mathbf{w}_T \doteq [w_T^1, \dots, w_T^K]$  belong to  $\Delta^K$  (the  $K - 1$  probability simplex).

- *Probabilistic Classifier Discrepancy:* For a distribution  $\mathcal{D}$ , we define the discrepancy between two functions  $f$  and  $g$  as:

$$\gamma_{\mathcal{D}}(f, g) = \mathbb{E}_{x \sim \mathcal{D}} [|f(x) - g(x)|]$$

We use  $g_T$  and  $g_S$  to represent the true labeling functions of the target and source domains, respectively. We use  $\gamma_S(f) \doteq \gamma_{P_S}(f, g_S)$  and  $\gamma_T(f) \doteq \gamma_{P_T}(f, g_T)$  to respectively denote the discrepancies of a hypothesis  $f$  to the true labeling function for the source and target domains.

- *Wasserstein Distance:* The Kantorovich-Rubenstein dual representation of the Wasserstein-1 distance between  $P_S$  and  $P_T$  can be written as (Villani, 2009):

$$W_1(P_S, P_T) = \sup_{\|f\|_L \leq 1} \mathbb{E}_{P_S}[f(x)] - \mathbb{E}_{P_T}[f(x)]$$

where the supremum is taken over all Lipschitz functions  $f$  with Lipschitz constant  $L \leq 1$  (referred to as the set of 1-Lipschitz functions).

For notational simplicity, we use  $D(X_1, X_2)$  to denote the distance between the distributions of any pair of random variables  $X_1$  and  $X_2$ . For instance,  $W_1(\Phi(X_S), \Phi(X_T))$  denotes the Wasserstein-1 distance between the distributions of the random variables  $\Phi(X_S)$  and  $\Phi(X_T)$  for any transformation  $\Phi$ .

## 4. Theory

The importance of the proposed generalization bounds in this section is two-fold: (1) they are theoretically proved to be at least as strong as existing popular upper bounds used in the literature (see Theorem 4.10) and are frequently much stronger on real-world data; (2) they inspire a new framework (see Section 5) that achieves state-of-the-art performance on both UDA benchmarks and real-world domain adaptation tasks (see Section 6).

### 4.1. Generalization Bounds for Domain Adaptation

Before presenting our theoretical results about sub-domain-based domain adaptation, we first present an upper bound closely related to the work of Ben-David et al. (2010) and Li et al. (2018). It is worth noting that we use the Wasserstein-1 distance in our analysis, as it provides a stronger bound than the total variation distance (Redko et al., 2017) employed by (Ben-David et al., 2010) [Theorem 1].

**Theorem 4.1** (Overall Generalization Bound). *For a hypothesis  $f : \mathcal{X} \rightarrow [0, 1]$ ,*

$$\gamma_T(f) \leq \gamma_S(f) + (\lambda + \lambda_H) W_1(P_S, P_T) + \gamma^* \quad (1)$$

where  $\gamma^* = \min_{f \in \mathbb{H}} \gamma_S(f) + \gamma_T(f)$ ,  $\mathbb{H}$  is a hypothesis class included in the set of  $\lambda_H$ -Lipschitz functions, and the true functions  $g_T$  and  $g_S$  are both  $\lambda$ -Lipschitz functions (as defined in Appendix A.1).

*Proof.* See in Appendix A.2.

**Remark 4.2.** The upper bound in Theorem 4.1 consists of three components: (i)  $\gamma_S(f)$  is the performance of the hypothesis on the source domain, (ii)  $W_1(P_S, P_T)$  is the distance between the source and the target domains, and (iii)  $\gamma^*$  is a constant that is related to the fundamental difference between the source and the target problems.

**Remark 4.3.** For succinctness and clarity of the following analysis, we assume without loss of generality that  $\lambda + \lambda_H \leq 1$ , simplifying the bound to

$$\gamma_T(f) \leq \gamma_S(f) + W_1(P_S, P_T) + \gamma^* \quad (2)$$

Numerous works attempt to solve the transfer learning problem by designing algorithms that attempt to minimize similar generalization bounds (e.g., Theorem 1 of Ben-David et al. (2010)). This approach first requires (1) selecting a mapping  $\Phi : \mathcal{X} \rightarrow \mathcal{H}$  to transform the original problem by mapping  $X_S$  and  $X_T$  into a shared hidden space  $\mathcal{H}$ , and (2) a hypothesis  $h : \mathcal{H} \rightarrow [0, 1]$  for prediction. Since  $\gamma_T(h \circ \Phi) = \gamma_{\Phi(X_T)}(h)$ , with Theorem 4.1, we can have a generalization bound for the performance of the function  $h \circ \Phi : \mathcal{X} \rightarrow [0, 1]$  on the original target problem:

$$\begin{aligned} \gamma_T(h \circ \Phi) &= \gamma_{\Phi(X_T)}(h) \\ &\leq \gamma_{\Phi(X_S)}(h) + W_1(\Phi(X_S), \Phi(X_T)) + \gamma_{\Phi}^*. \end{aligned} \quad (3)$$

If the distance between  $\Phi(X_S)$  and  $\Phi(X_T)$ , i.e.,  $W_1(\Phi(X_S), \Phi(X_T))$ , is close and the classification error of  $h$  on the transformed source problem, i.e.,  $\gamma_{\Phi(X_S)}(h)$ , remains low, then the performance of the hypothesis  $h \circ \Phi$  on the *original* target problem can be guaranteed.

This motivation has led to numerous domain adaptation frameworks that optimize the following objective

$$\min_{\substack{\Phi: \mathcal{X} \rightarrow \mathcal{H} \\ h: \mathcal{H} \rightarrow [0, 1]}} \gamma_{\Phi(X_S)}(h) + \alpha D(\Phi(X_S), \Phi(X_T)) \quad (4)$$

where  $\gamma_{\Phi(X_S)}(h)$  is the classification error of  $h$  on the transformed source problem,  $D$  is some distance between distributions and  $\alpha$  is the balancing weight. In this work, we consider the case where  $D$  is Wasserstein-1 distance.

## 4.2. Sub-domain-based Generalization Bounds for Domain Adaptation with Shifted Class Distribution

When taking the sub-domain information into consideration, we can have a stronger bound than the one in Theorem 4.1.

We first present several results that will be used to build toward the main theorem. These results themselves may be of interest. First of all, for each subdomain, Theorem 4.1 directly leads to the following Proposition:

**Proposition 4.4** (Sub-domain Generalization Bound). *For  $k \in \{1, \dots, K\}$ , where  $K$  represents the number of distinct subdomains, for sub-domain  $X_S^k$  with distribution  $P_S^k$  and  $X_T^k$  with distribution  $P_T^k$ , it holds any  $f \in \mathbb{H}$  that*

$$\gamma_T^k(f) \leq \gamma_S^k(f) + W_1(P_S^k, P_T^k) + (\gamma^k)^* \quad (5)$$

where  $(\gamma^k)^* = \min_{f \in \mathbb{H}} \gamma_S^k(f) + \gamma_T^k(f)$  is the minimum error can be reached,  $\mathbb{H}$  is a hypothesis class included in the set of  $\lambda_H$ -Lipschitz functions, the true functions  $g_T$  and  $g_S$  are both  $\lambda$ -Lipschitz functions, and  $\lambda + \lambda_H \leq 1$ .

Our second result shows that the classification error of any hypothesis  $f$  on a domain can be represented by a weighted sum of the classification errors of  $f$  on its sub-domains.

**Lemma 4.5** (Decomposition of the Classification Error). *For any hypothesis  $f \in \mathbb{H}$ ,*

$$\begin{aligned} \gamma_S(f) &= \sum_{k=1}^K w_S^k \gamma_S^k(f), \\ \gamma_T(f) &= \sum_{k=1}^K w_T^k \gamma_T^k(f). \end{aligned} \quad (6)$$

With Proposition 4.4 and Lemma 4.5, we can have a generalization bound of the target domain with sub-domain information:

**Theorem 4.6** (Sub-domain-based Generalization Bound).

$$\begin{aligned} \gamma_T(f, g_T) &\leq \sum_{k=1}^K w_T^k \gamma_S^k(f, g_S) \\ &\quad + \sum_{k=1}^K w_T^k W_1(P_S^k, P_T^k) + \sum_{k=1}^K w_T^k (\gamma^k)^* \end{aligned} \quad (7)$$

*Proof.* See in Appendix A.4.

We next show that, under reasonable assumptions, the weighted sum of distances between corresponding sub-domains of the source and target domains is at most as large as the distance between the marginal distribution of the source domain and that of the target domain.

**Theorem 4.7.** *If the following assumptions hold,*

- For  $k \in \{1, \dots, K\}$ ,  $P_S^k / P_T^k$  are Gaussian distributions with mean  $m_S^k / m_T^k$  and covariance  $\Sigma_S^k / \Sigma_T^k$ .
- The distance between the paired source-target sub-domain is smaller or equal to the distance between the non-paired source-target sub-domain, i.e., for  $k \neq k'$ , we have  $W_1(P_S^k, P_T^k) \leq W_1(P_S^k, P_T^{k'})$ .
- There exists an assumed small constant  $\epsilon > 0$ , such that  $\max_{1 \leq k \leq K} (\text{trace}(\Sigma_S^k)) \leq \epsilon$  and  $\max_{1 \leq k \leq K} (\text{trace}(\Sigma_T^{k'})) \leq \epsilon$ .



Then

$$\sum_{k=1}^K w_T^k W_1(P_S^k, P_T^k) \leq W_1(P_S, P_T) + \delta_c$$

where  $\delta_c$  is  $4\sqrt{\epsilon}$ .

*Proof.* See in Appendix A.8.

**Remark 4.8.**  $\delta_c$  is a constant dependent only on the variance of the features but not the covariance between features in different dimensions. Moreover, the inequality still holds without  $\delta_c$  on the right-hand side as demonstrated by our numerical experiments. To make our bound stronger, we add an intra-clustering loss  $\mathcal{L}_{intra}$  in our learning objectives to minimize the  $\delta_c$  term (details provided in Section 5.1.3).

**Remark 4.9.** The assumption of a Gaussian distribution for  $X^k$  is not unreasonable since it is often the result of a complex transformation,  $\Phi$ , and the Central Limit Theorem indicates that the outcome of such a transformation converges to a Gaussian distribution.

In the setting of shifted class distributions,  $w_T^k$  and  $w_S^k$  can be vastly different. To overcome this, we propose to minimize an objective with the simple intuition that *important sub-domains in the target domain need more attention*. With this motivation, we propose the following objective function for UDA with shifted class distribution:

$$\mathcal{L}(f) = \sum_{k=1}^K w_T^k \gamma_S^k(f). \quad (8)$$

In other words,  $\mathcal{L}$  reweights the sub-domains losses so that the subdomain with more weight in the target domain can be emphasized more.

We prove that in UDA with shifted class distributions, the sub-domain-based generalization bound is at least as strong as the general upper bound without sub-domain information as demonstrated by the following Theorem.

**Theorem 4.10.** Let  $\mathbb{H} \doteq \{f|f : \mathcal{X} \rightarrow [0, 1]\}$  denote a hypothesis space. Under the Assumptions in Theorem 4.7, if the following assumption hold for all  $f \in \mathbb{H}$ :

$$\sum_{k=1}^K w_T^k \gamma_S^k(f) \leq \sum_{k=1}^K w_S^k \gamma_S^k(f), \quad (9)$$

then we have

$$\sum_{k=1}^K w_T^k (\gamma^k)^* \leq \gamma^*.$$

Further, let

$$\begin{aligned} \epsilon_c(f) \doteq & \sum_{k=1}^K w_T^k \gamma_S^k(f, g_S) \\ & + \sum_{k=1}^K w_T^k W_1(P_S^k, P_T^k) + \sum_{k=1}^K w_T^k (\gamma^k)^* \end{aligned}$$

denote the sub-domain-based generalization bound, let

$$\epsilon_g(f) \doteq \gamma_S(f, g_S) + W_1(P_S, P_T) + \gamma^*$$

denote the general generalization bound without any sub-domain information. We have for all  $f$ ,

$$\epsilon_c(f) \leq \epsilon_g(f) + \delta_c$$

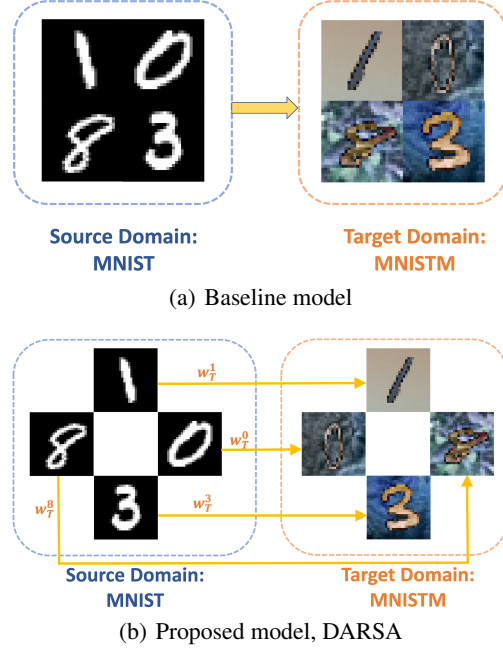


Figure 2. Figure 2(a): classic UDA methods. Figure 2(b): DARSA.  $w_T^k$  is the weight (i.e.,  $\mathbb{P}(y_T = k)$ ) of the  $k$ -th subdomain in target domain.

*Proof.* See in Appendix A.9.

**Remark 4.11.** We note that Assumption (9) is likely to hold, as we are minimizing the left hand side of Eq. (9).

**Remark 4.12.** In addition to theoretically proving that our proposed bound is at least as strong as the existing bound, we empirically observe that the sub-domain-based bound tends to be much stronger (see Figure 1 (b) and quantitative results in Section 6.1).

Inspired by Theorem 4.10, we next propose a framework for imbalanced UDA with the name *Domain Adaptation with Rebalanced Sub-domain Alignment* (DARSA for short).

## 5. Methods

Our proposed method, DARSA, focuses on aligning the distributions of the source and target sub-domains (Figure 2(b)) rather than matching the marginal distributions (Figure 2(a)). In DARSA, we divide the source domains into sub-domains based on class labels, and divide target domains into sub-domains using predicted class labels (serving as pseudo labels which have shown success in previous research (Lee et al., 2013; Deng et al., 2019)) for unlabeled target domains. This encourages homogeneous sub-domains (e.g., sub-domains with the same class labels in a classification task) to merge, while separating heterogeneous sub-domains for better decision boundaries.

Motivated by Theorem 4.6, the framework of DARSA,

shown in Figure 3, is composed of a source encoder  $f_E^S$  (parameterized by  $\theta_E^S$ ), a target encoder  $f_E^T$  (parameterized by  $\theta_E^T$ ), and a label classifier  $f_Y$  (parameterized by  $\theta_Y$ ). In our implementation, all three functions are defined as neural networks. We first pretrain  $f_E^S$  and  $f_Y$  with source data, and initialize  $f_E^S$  and  $f_E^T$  with pretrained weights. The source/target encoder  $f_E^S/f_E^T$  maps data to feature space, then the classifier  $f_Y$  uses extracted features to predict labels. Our framework is outlined in pseudo-code in Appendix B. Source labels and predicted target labels are used in the learning objective function for the following purposes: (i) Aligning the sub-domains of the source and the target; (ii) Estimating weights  $w_S$  and  $w_T$ ; (iii) Calculating weighted classification loss and clustering losses. We next give a detailed discussion of the learning objective function.

### 5.1. Learning Objectives

Our learning objectives are motivated by Theorem 4.6. Based on Equations 11, 12, 13, and 5.1.3, we can represent the learning objectives as follows:

$$\min_{\theta_Y, \theta_E^S, \theta_E^T} \lambda_Y \mathcal{L}_Y + \lambda_D \mathcal{L}_D + \mathcal{L}_C \quad (10)$$

where  $\mathcal{L}_Y$  represents weighted source domain classification error,  $\mathcal{L}_D$  represents weighted source-target domain discrepancy,  $\mathcal{L}_C = \lambda_c \mathcal{L}_{intra} + \lambda_a \mathcal{L}_{inter}$  represents the clustering loss (details provided in Section 5.1.3), and  $\lambda_Y$ ,  $\lambda_D$ ,  $\lambda_c$  and  $\lambda_a$  are hyperparameters representing weights of each loss. We next elaborate on each one of the losses.

#### 5.1.1. $\mathcal{L}_Y$ (WEIGHTED SOURCE DOMAIN CLASSIFICATION ERROR)

The weighted source domain classification error in Theorem 4.6 can be further expressed as:

$$\begin{aligned} & \sum_{k=1}^K w_T^k (\gamma_S^k(f, g_S)) \\ &= \sum_{k=1}^K w_T^k \int P_S(x|c=k) |f(x) - g_S(x)| dx \\ &= \sum_{k=1}^K w_T^k \int \frac{P_S(c=k|x) P_S(x)}{P_S(c=k)} |f(x) - g_S(x)| dx \\ &= \sum_{k=1}^K \frac{w_T^k}{w_S^k} \mathbb{E}_{x \sim D_S} w_S^k(x) |f(x) - g_S(x)| \end{aligned} \quad (11)$$

where variable  $c$  represents class,  $w_T^k = P_T(c=k)$ ,  $w_S^k = P_S(c=k)$ ,  $w_S^k(x) = P_S(c=k|x)$ . We say that  $P_S(c=k|x) = 1$  only when data point  $x$  is in class  $k$ , otherwise  $P_S(c=k|x) = 0$ .  $w_S^k$  can be set to the marginal source label distribution, and  $w_T^k$  can be estimated from the target predictions.

From Equation 11, we can express the empirical weighted source domain classification error as:

$$\mathcal{L}_Y(\theta_Y, \theta_E^S) = \frac{1}{N_S} \sum_{x^i \in \mathcal{X}_S} \mathbb{1}_{y^i=k} \frac{w_T^k}{w_S^k} \ell(\hat{y}^i, y^i)$$

where  $\hat{y}^i = f_Y(f_E^S(x^i))$  is the predicted label and  $\ell$  can be

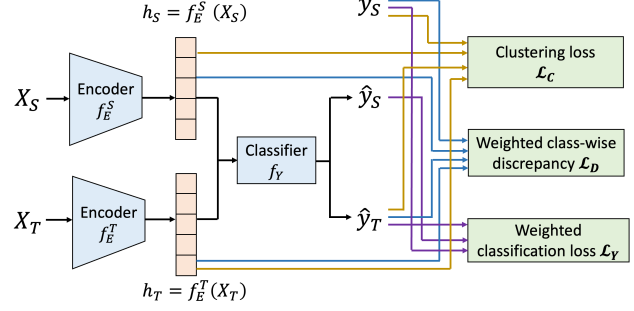


Figure 3. The DARS framework. Yellow lines representing the clustering loss  $\mathcal{L}_C$ , blue lines indicating domain discrepancy  $\mathcal{L}_D$ , and purple lines indicating source classification loss  $\mathcal{L}_Y$ .

any non-negative loss function (e.g., cross-entropy loss for classification tasks).

#### 5.1.2. $\mathcal{L}_D$ (WEIGHTED SOURCE-TARGET DOMAIN DISCREPANCY)

The weighted source-target domain discrepancy in Theorem 4.6 can be further expressed as:

$$\begin{aligned} \mathcal{L}_D(\theta_E^S, \theta_E^T, \theta_Y) &= \sum_{k=1}^K w_T^k W_1(P_S^k, P_T^k) \\ &= \sum_{k=1}^K w_T^k W_1(f_E^S(x_S^k), f_E^T(x_T^k)) \end{aligned} \quad (12)$$

where  $x_S^k$  are source samples with labels  $y_S = k$ ,  $x_T^k$  are target samples with predicted labels  $\hat{y}_T = k$ . In addition, we leverage the Sinkhorn algorithm (Cuturi, 2013) to approximate the Wasserstein metric.

#### 5.1.3. $\mathcal{L}_C$ (CLUSTERING LOSS)

Inspired by CAT (Deng et al., 2019), the clustering loss  $\mathcal{L}_C$  consists of two losses: the *intra-clustering loss*  $\mathcal{L}_{intra}$  and the *inter-clustering loss*  $\mathcal{L}_{inter}$ .

$\mathcal{L}_{intra}$  was first proposed to direct features of the same label to concentrate as well as to push features of different labels to separate from each other with at least a user-specified distance  $m$  (Luo et al., 2018). We use the following definition of  $\mathcal{L}_c$ :

$$\begin{aligned} \mathcal{L}_{intra}(\theta_E^S, \theta_E^T, \theta_Y) \\ = \mathcal{L}_{intra}(f_E^S(\mathcal{X}_S)) + \mathcal{L}_{intra}(f_E^T(\mathcal{X}_T)) \end{aligned} \quad (13)$$

with

$$\begin{aligned} \mathcal{L}_{intra}(f_E^S(\mathcal{X})) \\ = \frac{1}{N^2} \sum_{i,j=1}^N \left[ \delta_{ij} \|f_E(x_i) - f_E(x_j)\|^2 \right. \\ \left. + (1 - \delta_{ij}) \max(0, m - \|f_E(x_i) - f_E(x_j)\|)^2 \right] \end{aligned}$$

Table 1. Summary of UDA results on the digits datasets with shifted class distribution, measured in terms of prediction accuracy (%) on the target domain.

	MNIST to MNIST-M	MNISTM to MNIST	USPS to MNIST	SVHN to MNIST
DANN (Ganin et al., 2016)	63.1	93.0	59.8	64.9
WDGRL (Shen et al., 2018)	60.4	93.6	63.9	64.3
DSN (Bousmalis et al., 2016)	62.3	98.4	59.9	15.2
ADDA (Tzeng et al., 2017)	88.2	90.7	44.8	42.4
CAT (Deng et al., 2019)	54.1	95.4	81.0	65.8
CDAN (Long et al., 2018)	58.7	96.0	42.0	38.3
pixelDA (Bousmalis et al., 2017)	95.0	96.0	72.0	68.0
DRANet (Lee et al., 2021)	95.2	97.8	86.5	40.2
Source Only	47.9	91.5	40.8	53.7
<b>DARSA</b>	<b>96.0</b>	<b>98.8</b>	<b>92.6</b>	<b>90.1</b>

where  $N$  represents the number of samples in the domain  $\mathcal{X}$ ,  $\delta_{ij} = 1$  only if  $x_i$  and  $x_j$  have the same label (using ground truth label in source domain; use predicted label in target domain), otherwise  $\delta_{ij} = 0$ .  $m$  is a pre-defined distance controlling how separate we want each class to be.

$\mathcal{L}_{inter}$  is leveraged to help domain adaptation by aligning centroids of the source sub-domains with that of the corresponding target sub-domains in the representation space. The definition of  $\mathcal{L}_{inter}$  is

$$\begin{aligned} \mathcal{L}_{inter}(\theta_E^S, \theta_E^T, \theta_Y) \\ = \frac{1}{K} \sum_{k=1}^K \|c(f_E^S(x_T^k)) - c(f_E^T(x_T^k))\|^2 \end{aligned} \quad (14)$$

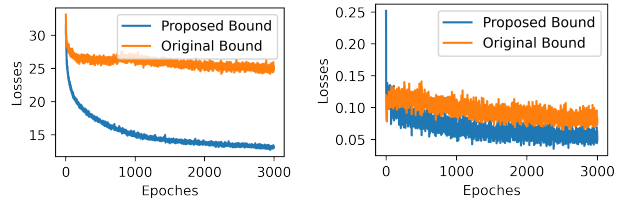
where  $c(\cdot)$  calculates the centroids of the sub-domains.

## 6. Results

We first demonstrate through empirical evidence that our proposed generalization bound is stronger. After that, we evaluate our proposed method, DARSA, on four benchmark UDA tasks using digit datasets and two tasks using real-world neural datasets. All source-target datasets are re-sampled to enforce shifted label distributions. We show that our method outperforms all state-of-the-art transfer learning methods under shifted label distributions, including methods specifically designed for computer vision tasks. As shown in Figure 5, our method learns a feature space that is discriminative and domain-invariant, resulting in improved performance in target domain predictions.

### 6.1. Empirical Analysis of our Proposed Generalization Bound

In our empirical analysis of our proposed generalization bound, we evaluate the bound on the MNIST to MNIST-M UDA task (dataset details in Section 6.2). As shown in



(a) Domain discrepancy (b) Source Classification Loss

Figure 4. For MNIST to MNIST-M UDA task with shifted class distribution, a) Compare the domain discrepancy term ( $\mathcal{L}_D$ ) in our proposed bound to that in Remark 4.3 b) Compare the source classification term ( $\mathcal{L}_Y$ ) in our proposed bound to that in 4.1

Figure 4, our empirical results demonstrate that our theory, i.e., Theorem 4.6 provides a stronger generalization bound than Theorem 4.1. Additional empirical results to support this claim are provided in Appendix C.2.

### 6.2. Experiments on Digit Datasets with Shifted Class Distribution

We conduct experiments on four digit datasets: MNIST (LeCun et al., 1998), MNIST-M (Ganin et al., 2016), USPS, and Street View House Numbers (SVHN) (Netzer et al., 2011). To create class distribution shifts, we subsample the datasets so that the proportion of odd digits is three times the proportion of even digits in the source dataset, and vice versa in the target dataset. To ensure a fair comparison, all methods use a subset of the labeled target domain data (around 1000 samples) as a validation set for the hyperparameters search. This validation set performance serves as an upper bound for evaluating the performance of UDA methods. The experimental details (dataset description, model structure and hyperparameters) are provided in appendix C.

As shown in Table 1, our model outperforms all competing methods. We note that most of the SOTA comparisons are not specifically designed for shifted class distribution scenarios, and this setting caused issues in several competing

Table 2. Summary of UDA results on the TST datasets with shifted class distribution, measured in terms of prediction accuracy (%) on the target domain.

	Bipolar to Wildtype	Wildtype to Bipolar
DANN (Ganin et al., 2016)	79.9	81.5
WDGRL (Shen et al., 2018)	79.6	79.5
DSN (Bousmalis et al., 2016)	79.4	80.9
ADDA (Tzeng et al., 2017)	75.1	72.6
CAT (Deng et al., 2019)	77.3	78.6
CDAN (Long et al., 2018)	75.0	73.6
Source Only	73.8	70.4
<b>DARSA</b>	<b>86.6</b>	<b>84.8</b>

methods. We use Adaptive Experimentation (Ax) platform (Bakshy et al.; Letham et al., 2019), an automatic tuning approach to select hyperparameters to maximize their performance in domain shifting scenarios (see Appendix C.4).

### 6.3. Experiments on the TST Dataset with Shifted Class Distribution

The Tail Suspension Test (TST) dataset (Gallagher et al., 2017) consists of local field potentials (LFPs) recorded from the brains of 26 mice. These mice belong to two genetic backgrounds: a genetic model of bipolar disorder (Clock- $\Delta$ 19) and wildtype mice. Each mouse is subjected to 3 behavioral assays which are designed to vary stress: home cage (HC), open field (OF), and tail-suspension (TS). We conduct experiments on two transfer learning tasks using these neural activity data: transferring from wildtype mice to the bipolar mouse model and vice versa. We aim to predict for each one second window which of the 3 conditions - HC, OF, or TS - the mouse is currently experiencing. To create class distribution shifts, we subsample the datasets so that we have 6000 Homeage observations, 3000 Open Field observations, and 6000 Tail Suspension observations in the bipolar genotype dataset and 3000 Homeage observations, 6000 OpenField observations, and 3000 Tail Suspension observations in the wildtype genotype dataset. The experimental details (dataset description, model structure and hyperparameters) are provided in appendix D. As shown in Table 2, our model outperforms all competing methods.

### 6.4. Analysis of Feature Space

We visualize the feature spaces learned by DANN (Ganin et al., 2016) and our method, DARSA, using UMAP (Sainburg et al., 2021). As shown in Figure 5 (a) and (b), features learned with DARSA form stronger clusters when the labels are the same, and clusters with different labels are more separated from one another. In contrast, DANN (Ganin et al., 2016) fails to learn a good source-target domain alignment in the feature space (shown in Figure 5 (c) and (d)) in the presence of class distribution shifts. This confirms that our

method, DARSA, can learn a class-conditional feature space that is discriminative and domain-invariant, which improves performance in target domain prediction.

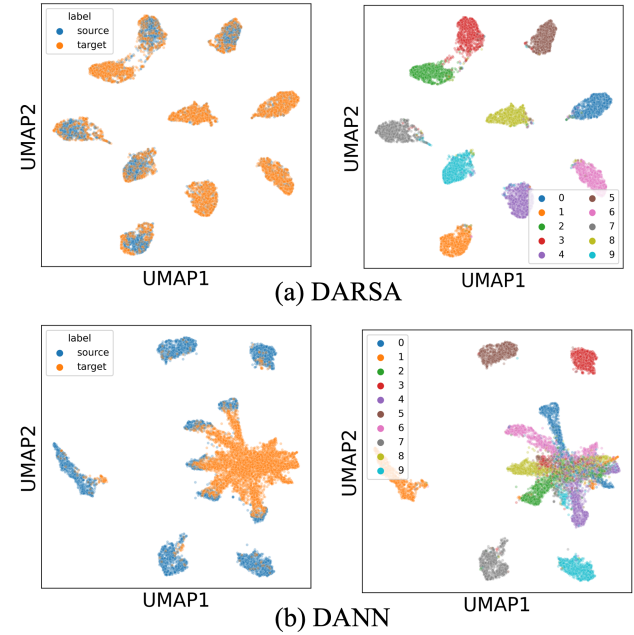


Figure 5. For MNIST to MNIST-M UDA task with shifted class distribution (a) feature space learned by our method, DARSA. (b) feature space learned by DANN. Left panel: colored by source/target; Right panel: colored by true label (digit). The features are projected to 2-D using UMAP.

## 7. Discussion and Conclusion

In this paper, we propose a novel bound for UDA that motivates a novel algorithm with improved performance in various tasks. Since most domain adaptation work is based on reducing the distribution gaps in the source and target domain without incorporating class-conditional structure, we address this challenge to improve alignment between domains during training. We show that our method outperforms state-of-the-art methods in class imbalance and class distribution shifting scenarios. Our work focuses on classification tasks with source and target having the same number of distinct classes; however, in some cases, this could be addressed by combining similar classes. In addition, by choosing an appropriate clustering algorithm within the framework, this work has the potential to extend to regression tasks. Our current method is also limited to two domains, and future work will extend our method to multiple domains. Lastly, Johansson et al. (2016) shows that estimating counterfactual outcomes in causal inference under ignorability is mathematically equivalent to UDA between domains  $D \in \{0, 1\}$  under covariate shift (Johansson et al., 2020). With the equivalency, our framework has the potential to be used in causal inference scenarios.



---

## References

- Arbelaez, P., Maire, M., Fowlkes, C., and Malik, J. Contour detection and hierarchical image segmentation. *IEEE transactions on pattern analysis and machine intelligence*, 33(5):898–916, 2010.
- Bakshy, E., Balandat, M., and Kashin, K. Open-sourcing ax and botorch: New ai tools for adaptive experimentation. URL <https://ai.facebook.com/blog/open-sourcing-ax-and-botorch-new-ai-tools-for-adaptive-experimentation>.
- Ben-David, S., Blitzer, J., Crammer, K., and Pereira, F. Analysis of representations for domain adaptation. *Advances in neural information processing systems*, 19, 2006.
- Ben-David, S., Blitzer, J., Crammer, K., Kulesza, A., Pereira, F., and Vaughan, J. W. A theory of learning from different domains. *Machine learning*, 79(1):151–175, 2010.
- Borgwardt, K. M., Gretton, A., Rasch, M. J., Kriegel, H.-P., Schölkopf, B., and Smola, A. J. Integrating structured biological data by kernel maximum mean discrepancy. *Bioinformatics*, 22(14):e49–e57, 2006.
- Bousmalis, K., Trigeorgis, G., Silberman, N., Krishnan, D., and Erhan, D. Domain separation networks. *Advances in neural information processing systems*, 29, 2016.
- Bousmalis, K., Silberman, N., Dohan, D., Erhan, D., and Krishnan, D. Unsupervised pixel-level domain adaptation with generative adversarial networks. In *Proceedings of the IEEE conference on computer vision and pattern recognition*, pp. 3722–3731, 2017.
- Chawla, N. V. Data mining for imbalanced datasets: An overview. *Data mining and knowledge discovery handbook*, pp. 875–886, 2009.
- Cuturi, M. Sinkhorn distances: Lightspeed computation of optimal transport. *Advances in neural information processing systems*, 26, 2013.
- Delon, J. and Desolneux, A. A wasserstein-type distance in the space of gaussian mixture models. *SIAM Journal on Imaging Sciences*, 13(2):936–970, 2020.
- Deng, Z., Luo, Y., and Zhu, J. Cluster alignment with a teacher for unsupervised domain adaptation. In *Proceedings of the IEEE/CVF international conference on computer vision*, pp. 9944–9953, 2019.
- Farahani, A., Voghoei, S., Rasheed, K., and Arabnia, H. R. A brief review of domain adaptation. *Advances in data science and information engineering*, pp. 877–894, 2021.
- Fournier, N. and Guillin, A. On the rate of convergence in wasserstein distance of the empirical measure. *Probability Theory and Related Fields*, 162(3):707–738, 2015.
- Gallagher, N., Ulrich, K. R., Talbot, A., Dzirasa, K., Carin, L., and Carlson, D. E. Cross-spectral factor analysis. *Advances in neural information processing systems*, 30, 2017.
- Ganin, Y. and Lempitsky, V. Unsupervised domain adaptation by backpropagation. In *International conference on machine learning*, pp. 1180–1189. PMLR, 2015.
- Ganin, Y., Ustinova, E., Ajakan, H., Germain, P., Larochelle, H., Laviolette, F., Marchand, M., and Lempitsky, V. Domain-adversarial training of neural networks. *The journal of machine learning research*, 17(1):2096–2030, 2016.
- Gulrajani, I., Ahmed, F., Arjovsky, M., Dumoulin, V., and Courville, A. C. Improved training of wasserstein gans. *Advances in neural information processing systems*, 30, 2017.
- HassanPour Zonoozi, M. and Seydi, V. A survey on adversarial domain adaptation. *Neural Processing Letters*, pp. 1–41, 2022.
- Hoffman, J., Tzeng, E., Park, T., Zhu, J.-Y., Isola, P., Saenko, K., Efros, A., and Darrell, T. Cycada: Cycle-consistent adversarial domain adaptation. In *International conference on machine learning*, pp. 1989–1998. Pmlr, 2018.
- Isola, P., Zhu, J.-Y., Zhou, T., and Efros, A. A. Image-to-image translation with conditional adversarial networks. In *Proceedings of the IEEE conference on computer vision and pattern recognition*, pp. 1125–1134, 2017.
- Japkowicz, N. and Stephen, S. The class imbalance problem: A systematic study. *Intelligent data analysis*, 6(5):429–449, 2002.
- Jiang, X., Lao, Q., Matwin, S., and Havaei, M. Implicit class-conditioned domain alignment for unsupervised domain adaptation. In *International Conference on Machine Learning*, pp. 4816–4827. PMLR, 2020.
- Johansson, F., Shalit, U., and Sontag, D. Learning representations for counterfactual inference. In *International conference on machine learning*, pp. 3020–3029. PMLR, 2016.
- Johansson, F. D., Shalit, U., Kallus, N., and Sontag, D. Generalization bounds and representation learning for estimation of potential outcomes and causal effects. *arXiv preprint arXiv:2001.07426*, 2020.

- 
- LeCun, Y., Bottou, L., Bengio, Y., and Haffner, P. Gradient-based learning applied to document recognition. *Proceedings of the IEEE*, 86(11):2278–2324, 1998.
- Lee, D.-H. et al. Pseudo-label: The simple and efficient semi-supervised learning method for deep neural networks. In *Workshop on challenges in representation learning, ICML*, volume 3, pp. 896, 2013.
- Lee, S., Cho, S., and Im, S. Dranet: Disentangling representation and adaptation networks for unsupervised cross-domain adaptation. In *Proceedings of the IEEE/CVF conference on computer vision and pattern recognition*, pp. 15252–15261, 2021.
- Letham, B., Karrer, B., Ottoni, G., and Bakshy, E. Constrained bayesian optimization with noisy experiments. 2019.
- Li, X., Yu, L., Chen, H., Fu, C.-W., Xing, L., and Heng, P.-A. Transformation-consistent self-ensembling model for semisupervised medical image segmentation. *IEEE Transactions on Neural Networks and Learning Systems*, 32(2):523–534, 2020.
- Li, Y., Carlson, D. E., et al. Extracting relationships by multi-domain matching. *Advances in Neural Information Processing Systems*, 31, 2018.
- Liang, K. J., Li, C., Wang, G., and Carin, L. Generative adversarial network training is a continual learning problem. *arXiv preprint arXiv:1811.11083*, 2018.
- Liu, M.-Y., Breuel, T., and Kautz, J. Coupled generative adversarial networks. *arXiv preprint arXiv:1606.07536*, 2016.
- Long, M., Cao, Y., Wang, J., and Jordan, M. Learning transferable features with deep adaptation networks. In *International conference on machine learning*, pp. 97–105. PMLR, 2015.
- Long, M., Cao, Z., Wang, J., and Jordan, M. I. Conditional adversarial domain adaptation. *Advances in neural information processing systems*, 31, 2018.
- Lu, L., Zheng, Y., Carneiro, G., and Yang, L. Deep learning and convolutional neural networks for medical image computing. *Advances in computer vision and pattern recognition*, 10:978–3, 2017.
- Lu, Y. and Lu, J. A universal approximation theorem of deep neural networks for expressing probability distributions. *Advances in neural information processing systems*, 33: 3094–3105, 2020.
- Luo, Y., Zhu, J., Li, M., Ren, Y., and Zhang, B. Smooth neighbors on teacher graphs for semi-supervised learning. In *Proceedings of the IEEE conference on computer vision and pattern recognition*, pp. 8896–8905, 2018.
- Mansour, Y., Mohri, M., and Rostamizadeh, A. Multiple source adaptation and the rényi divergence. *arXiv preprint arXiv:1205.2628*, 2012.
- Netzer, Y., Wang, T., Coates, A., Bissacco, A., Wu, B., and Ng, A. Y. Reading digits in natural images with unsupervised feature learning. 2011.
- Peng, K.-C., Wu, Z., and Ernst, J. Zero-shot deep domain adaptation. In *Proceedings of the European Conference on Computer Vision (ECCV)*, pp. 764–781, 2018.
- Pinheiro, P. O. Unsupervised domain adaptation with similarity learning. In *Proceedings of the IEEE conference on computer vision and pattern recognition*, pp. 8004–8013, 2018.
- Redko, I., Habrard, A., and Sebban, M. Theoretical analysis of domain adaptation with optimal transport. In *Joint European Conference on Machine Learning and Knowledge Discovery in Databases*, pp. 737–753. Springer, 2017.
- Sainburg, T., McInnes, L., and Gentner, T. Q. Parametric umap embeddings for representation and semisupervised learning. *Neural Computation*, 33(11):2881–2907, 2021.
- Sankaranarayanan, S., Balaji, Y., Jain, A., Lim, S. N., and Chellappa, R. Learning from synthetic data: Addressing domain shift for semantic segmentation. In *Proceedings of the IEEE conference on computer vision and pattern recognition*, pp. 3752–3761, 2018.
- Shen, J., Qu, Y., Zhang, W., and Yu, Y. Wasserstein distance guided representation learning for domain adaptation. In *Proceedings of the AAAI Conference on Artificial Intelligence*, volume 32, 2018.
- Shi, Y. and Sha, F. Information-theoretical learning of discriminative clusters for unsupervised domain adaptation. *arXiv preprint arXiv:1206.6438*, 2012.
- Snell, J., Swersky, K., and Zemel, R. Prototypical networks for few-shot learning. *Advances in neural information processing systems*, 30, 2017.
- Sun, B., Feng, J., and Saenko, K. Return of frustratingly easy domain adaptation. In *Proceedings of the AAAI Conference on Artificial Intelligence*, volume 30, 2016.
- Tan, S., Peng, X., and Saenko, K. Generalized domain adaptation with covariate and label shift co-alignment. 2019.
- Tzeng, E., Hoffman, J., Zhang, N., Saenko, K., and Darrell, T. Deep domain confusion: Maximizing for domain invariance. *arXiv preprint arXiv:1412.3474*, 2014.

- 
- Tzeng, E., Hoffman, J., Darrell, T., and Saenko, K. Simultaneous deep transfer across domains and tasks. In *Proceedings of the IEEE international conference on computer vision*, pp. 4068–4076, 2015.
- Tzeng, E., Hoffman, J., Saenko, K., and Darrell, T. Adversarial discriminative domain adaptation. In *Proceedings of the IEEE conference on computer vision and pattern recognition*, pp. 7167–7176, 2017.
- Tzeng, E., Devin, C., Hoffman, J., Finn, C., Abbeel, P., Levine, S., Saenko, K., and Darrell, T. Adapting deep visuomotor representations with weak pairwise constraints. In *Algorithmic Foundations of Robotics XII*, pp. 688–703. Springer, 2020.
- Villani, C. *Optimal transport: old and new*, volume 338. Springer, 2009.
- Wang, M. and Deng, W. Deep visual domain adaptation: A survey. *Neurocomputing*, 312:135–153, 2018.

## A. Definitions and Proofs

**Definition A.1.** For some  $K \geq 0$ , the set of  $K$ -Lipschitz functions denotes the set of functions  $f$  that verify:

$$\|f(x) - f(x')\| \leq K\|x - x'\|, \forall x, x' \in \mathcal{X}$$

In the coming proofs, we assume that the hypothesis class  $\mathbb{H}$  is a subset of  $\lambda_H$ -Lipschitz functions, where  $\lambda_H$  is a positive constant, and we assume that the true labeling functions are  $\lambda$ -Lipschitz for some positive real number  $\lambda$ .

**Theorem A.2** (Overall Generalization Bound (Theorem A.8 in (Li et al., 2018))). *For a hypothesis  $f \in \mathbb{H}$*

$$\gamma_T(f, g_T) \leq \gamma_S(f, g_S) + (\lambda + \lambda_H)W_1(P_S, P_T) + \gamma^* \quad (15)$$

where  $\gamma^* = \min_{f \in \mathbb{H}} \gamma_S(f) + \gamma_T(f)$  measures how fundamentally different the true labels are for the two domains.

*Proof.* Let  $f$  be a hypothesis function in  $\mathbb{H}$ , we have that

$$\gamma_T(f, g_T) = \gamma_T(f, g_T) + \gamma_S(f, g_S) - \gamma_S(f, g_S) + \gamma_S(f, g_T) - \gamma_S(f, g_T) \quad (16)$$

And then bound the output term by taking the absolute value of differences:

$$\begin{aligned} \gamma_T(f, g_T) &\leq \gamma_S(f, g_S) + |\gamma_S(f, g_T) - \gamma_S(f, g_S)| + |\gamma_T(f, g_T) - \gamma_S(f, g_T)| \\ &\leq \gamma_S(f, g_S) + \mathbb{E}_{X_S}[|g_S(x) - g_T(x)|] + |\gamma_T(f, g_T) - \gamma_S(f, g_T)| \end{aligned} \quad (17)$$

As stated in (Li et al., 2018)), the first two terms proceed exactly as by (Ben-David et al., 2010); further derivations are not provided. Let  $P_S$  and  $P_T$  be the densities of  $X_S$  and  $X_T$ , respectively.

$$|\gamma_T(f, g_T) - \gamma_S(f, g_T)| \leq \left| \int (P_T(x) - P_S(x))|f(x) - g_T(x)|dx \right| \quad (18)$$

Since our hypothesis class  $\mathbb{H}$  is assumed to be  $\lambda_H$ -Lipschitz and the true labeling functions are  $\lambda$ -Lipschitz, we have that for every function  $f \in \mathbb{H}$ ,  $h : x \mapsto |f(x) - g_T(x)|$  is  $\lambda + \lambda_H$ -Lipschitz and it takes its values in  $[0, 1]$ . Therefore,

$$\begin{aligned} |\gamma_T(f, g_T) - \gamma_S(f, g_T)| &\leq \left| \sup_{h: \mathcal{X} \rightarrow [0,1], \|h\| \leq \lambda + \lambda_H} \int (P_T(x) - P_S(x))h(x)dx \right| \\ &= \left| \sup_{h: \mathcal{X} \rightarrow [0,1], \|h\| \leq \lambda + \lambda_H} (\mathbb{E}_{X_T}[h(x)] - \mathbb{E}_{X_S}[h(x)]) \right| \end{aligned} \quad (19)$$

Note that due to the symmetric nature of the function space (i.e if  $h$  is  $K$ -Lipschitz then  $-h$  is  $K$ -Lipschitz) we can just pick either side to lead with and drop the absolute value, yielding

$$|\gamma_T(f, g_T) - \gamma_S(f, g_T)| \leq \left| \max_{h: \mathcal{X} \rightarrow [0,1], \|h\| \leq \lambda + \lambda_H} (\mathbb{E}_{X_T}[h(x)] - \mathbb{E}_{X_S}[h(x)]) \right| \leq (\lambda + \lambda_H)W_1(P_S, P_T) \quad (20)$$

Following the Theorem 2 of Ben-David et al. (2010), we can also easily bound the target error  $\gamma_T(f, g_T)$  by:

$$\gamma_T(f, g_T) \leq \gamma_S(f, g_S) + (\lambda + \lambda_H)W_1(P_S, P_T) + \gamma^* \quad (21)$$

where  $\gamma^* = \min_{f \in \mathbb{H}} \gamma_S(f, g_S) + \gamma_T(f, g_T)$  is the minimum error can be reached.

**Lemma A.3** (Decomposition of the Classification Error). *For any hypothesis  $f \in \mathbb{H}$ ,*

$$\begin{aligned} \gamma_S(f) &= \sum_{k=1}^K w_S^k \gamma_S^k(f), \\ \gamma_T(f) &= \sum_{k=1}^K w_T^k \gamma_T^k(f). \end{aligned} \quad (22)$$



*Proof.* We can write out  $\gamma_S(f, g_S)$  as clustering specific component. Here we use  $c$  to represent the clustering index.

$$\begin{aligned}
\gamma_S(f, g_S) &= \mathbb{E}_{X_S} [|f(x) - g_S(x)|] \\
&= \int P_S(x) |f(x) - g_S(x)| dx \\
&= \int \sum_{k=1}^K w_S^k P_S(x|c=k) |f(x) - g_S(x)| dx \\
&= \sum_{k=1}^K w_S^k \int P_S(x|c=k) |f(x) - g_S(x)| dx \\
&= \sum_{k=1}^K w_S^k \int P_S(x|c=k) |f(x) - g_S(x)| dx \\
&= \sum_{k=1}^K w_S^k \gamma_S^k(f, g_S)
\end{aligned} \tag{23}$$

With similar proof, we have:

$$\gamma_T(f, g_T) = \sum_{k=1}^K w_T^k \gamma_T^k(f, g_T) \tag{24}$$

**Theorem A.4** (Class-conditional Generalization Bound).

$$\gamma_T(f, g_T) \leq \sum_{k=1}^K w_T^k \gamma_S^k(f, g_S) + \sum_{k=1}^K w_T^k W_1(P_S^k, P_T^k) + \sum_{k=1}^K w_T^k (\gamma^k)^* \tag{25}$$

*Proof.*

$$\begin{aligned}
\gamma_T(f, g_T) &\stackrel{\text{Lemma 4.5}}{=} \sum_{k=1}^K w_T^k \gamma_T^k(f, g_T) \\
&\stackrel{\text{Proposition 4.4}}{\leq} \sum_{k=1}^K w_T^k \{ \gamma_S^k(f, g_S) + W_1(P_S^k, P_T^k) + (\gamma^k)^* \}
\end{aligned} \tag{26}$$

In Definition A.5, we define a Wasserstein-like distance between Gaussian Mixture Models, which uses Wasserstein-1 distance as a variation of the Proposition 4 in (Delon & Desolneux, 2020).

**Definition A.5** (Wasserstein-like distance between Gaussian Mixture Models). Assume  $P_S = \sum_{k=1}^K w_S^k P_S^k$  and  $P_T = \sum_{k=1}^K w_T^k P_T^k$  be two Gaussian mixtures. We define:

$$MW_1(P_S, P_T) = \min_{w \in \Pi(w_S, w_T)} \sum_{k=1}^K \sum_{k'=1}^K w_{k,k'} W_1(P_S^k, P_T^{k'}) \tag{27}$$

where  $\Pi(w_S, w_T)$  represents the simplex  $\Delta^{K \times K}$  with marginals  $w_S$  and  $w_T$ .

**Lemma A.6** (Extension to Wasserstein-1 - Lemma 4.1 of (Delon & Desolneux, 2020)). *Explicit the distance  $MW_1$  between a Gaussian mixture and a mixture of Dirac distributions. Let  $\mu_0 = \sum_{k=1}^{K_0} \pi_0^k \mu_0^k$  with  $\mu_0^k = \mathcal{N}(m_0^k, \Sigma_0^k)$  and  $\mu_1 = \sum_{k=1}^{K_1} \pi_1^k \delta_{m_1^k}$ . Let  $\tilde{\mu}_0 = \sum_{k=1}^{K_0} \pi_0^k \delta_{m_0^k}$  ( $\tilde{\mu}_0$  only retains the means of  $\mu_0$ ). Then,*

$$MW_1(\mu_0, \mu_1) \leq W_1(\tilde{\mu}_0, \mu_1) + \sum_{k=1}^{K_0} \pi_0^k \sqrt{\text{tr}(\Sigma_0^k)}$$

*Proof.*

$$\begin{aligned}
MW_1(\mu_0, \mu_1) &= \inf_{w \in \Pi(\pi_0, \pi_1)} \sum_{k,l} w_{k,l} W_1(\mu_0^k, \delta_{m_1^l}) \\
&\leq \inf_{w \in \Pi(\pi_0, \pi_1)} \sum_{k,l} w_{k,l} W_2(\mu_0^k, \delta_{m_1^l}) \\
&= \inf_{w \in \Pi(\pi_0, \pi_1)} \sum_{k,l} w_{k,l} \left[ \sqrt{\|m_1^l - m_0^k\|^2 + \text{tr}(\Sigma_0^k)} \right] \\
&\leq \inf_{w \in \Pi(\pi_0, \pi_1)} \sum_{k,l} w_{k,l} \|m_1^l - m_0^k\| + \sum_k \pi_0^k \sqrt{\text{tr}(\Sigma_0^k)} \\
&\leq W_1(\tilde{\mu}_0, \mu_1) + \sum_{k=1}^{K_0} \pi_0^k \sqrt{\text{tr}(\Sigma_0^k)}
\end{aligned} \tag{28}$$

**Theorem A.7** (Extension to Wasserstein-1 - Proposition 6 of (Delon & Desolneux, 2020)). *Let  $P_S$  and  $P_T$  be two Gaussian mixtures. If for  $\forall k, k'$ , we assume  $\max_k(\text{trace}(\Sigma_S^k)) \leq \epsilon$  and  $\max_{k'}(\text{trace}(\Sigma_T^{k'})) \leq \epsilon$ . then:*

$$MW_1(P_S, P_T) \leq W_1(P_S, P_T) + 4\sqrt{\epsilon} \tag{29}$$

*Proof.* Here, we follow the same structure of the proof for Wasserstein-2 in (Delon & Desolneux, 2020). Let  $(P_S^n)_n$  and  $(P_T^n)_n$  be two sequences of mixtures of Dirac masses respectively converging to  $P_S$  and  $P_T$  in  $\mathcal{P}_1(\mathbb{R}^d)$ . Since  $MW_1$  is a distance,

$$\begin{aligned}
MW_1(P_S, P_T) &\leq MW_1(P_S^n, P_T^n) + MW_1(P_S, P_S^n) + MW_1(P_T, P_T^n) \\
&= W_1(P_S^n, P_T^n) + MW_1(P_S, P_S^n) + MW_1(P_T, P_T^n)
\end{aligned}$$

We can study the limits of these three terms when  $n \rightarrow +\infty$

First, observe that  $MW_1(P_S^n, P_T^n) = W_1(P_S^n, P_T^n) \xrightarrow{n \rightarrow +\infty} W_1(P_S, P_T)$  since  $W_1$  is continuous on  $\mathcal{P}_1(\mathbb{R}^d)$ .

Second, based on Lemma A.6, we have that

$$MW_1(P_S, P_S^n) = W_1(\tilde{P}_S, P_S^n) + \sum_{k=1}^K w_S^k \sqrt{\text{tr}(\Sigma_S^k)} \xrightarrow{n \rightarrow +\infty} W_1(\tilde{P}_S, P_S) + \sum_{k=1}^K w_S^k \sqrt{\text{tr}(\Sigma_S^k)}$$

We observe that  $x \mapsto \sqrt{x}$  is a concave function, thus by Jensen's inequality, we have that

$$\sum_{k=1}^K w_S^k \sqrt{\text{tr}(\Sigma_S^k)} \leq \sqrt{\sum_{k=1}^K w_S^k \text{tr}(\Sigma_S^k)}$$

Also By Jensen's inequality, we have that,

$$W_1(\tilde{P}_S, P_S) \leq W_2(\tilde{P}_S, P_S)$$

And from (Delon & Desolneux, 2020) we have that

$$W_2(\tilde{P}_S, P_S) \leq \sqrt{\sum_{k=1}^K w_S^k \text{tr}(\Sigma_S^k)}$$

Similarly for  $MW_1(P_T, P_T^n)$  the same argument holds. Therefore we have,

$$\lim_{n \rightarrow \infty} MW_1(P_S, P_S^n) \leq 2 \sqrt{\sum_{k=1}^K w_S^k \text{tr}(\Sigma_S^k)}$$

And

$$\lim_{n \rightarrow \infty} MW_1(P_T, P_T^n) \leq 2\sqrt{\sum_{k=1}^K w_S^k \text{tr}(\Sigma_S^k)}$$

We can conclude that:

$$\begin{aligned} MW_1(P_S, P_T) &\leq \lim_{n \rightarrow \infty} (W_1(P_S^n, P_T^n) + MW_1(P_S, P_S^n) + MW_1(P_T, P_T^n)) \\ &\leq W_1(P_S, P_T) + 2\sqrt{\sum_{k=1}^K w_S^k \text{tr}(\Sigma_S^k)} + 2\sqrt{\sum_{k=1}^K w_T^k \text{tr}(\Sigma_T^k)} \\ &\leq W_1(P_S, P_T) + 4\sqrt{\epsilon} \end{aligned}$$

This concludes the proof.

**Theorem A.8.** *If the following assumptions hold,*

- For  $k \in \{1, \dots, K\}$ ,  $P_S^k / P_T^k$  are Gaussian distributions with mean  $m_S^k / m_T^k$  and covariance  $\Sigma_S^k / \Sigma_T^k$ .
- The distance between the paired source-target sub-domain is smaller or equal to the distance between the non-paired source-target sub-domain, i.e., for  $k \neq k'$ , we have  $W_1(P_S^k, P_T^k) \leq W_1(P_S^k, P_T^{k'})$ .
- There exists a constant  $\epsilon > 0$ , such that  $\max_{1 \leq k \leq K} (\text{trace}(\Sigma_S^k)) \leq \epsilon$  and  $\max_{1 \leq k \leq K} (\text{trace}(\Sigma_T^k)) \leq \epsilon$ . This  $\epsilon$  is assumed to be reasonably small.

Then

$$\sum_{k=1}^K w_T^k W_1(P_S^k, P_T^k) \leq W_1(P_S, P_T)$$

which implies Theorem 4.6 provides a stronger source-target domain discrepancy term in the generalization bound than Theorem 4.1.

*Proof.* Since  $w \in \Pi(w_S, w_T)$ , we can write out  $w_T^k$  as  $\sum_{k'=1}^K w_{k,k'}$ , then based on assumption 2, we have:

$$\begin{aligned} \sum_{k=1}^K w_T^k W_1(P_S^k, P_T^k) &= \sum_{k=1}^K \sum_{k'=1}^K w_{k,k'} W_1(P_S^k, P_T^k) \\ &\leq \sum_{k=1}^K \sum_{k'=1}^K w_{k,k'} W_1(P_S^k, P_T^{k'}) \end{aligned}$$

Thus we have,

$$\begin{aligned} \sum_{k=1}^K w_T^k W_1(P_S^k, P_T^k) &\leq \min_{w \in \Pi(w_S, w_T)} \sum_{k=1}^K \sum_{k'=1}^K w_{k,k'} W_1(P_S^k, P_T^{k'}) \\ &= MW_1(P_S, P_T) \end{aligned} \tag{30}$$

Also we prove in Theorem A.7 that:

$$MW_1(P_S, P_T) \leq W_1(P_S, P_T) + 4\sqrt{\epsilon}$$

Then we conclude our proof and show that:

$$\sum_{k=1}^K w_T^k W_1(P_S^k, P_T^k) \leq MW_1(P_S, P_T) \leq W_1(P_S, P_T) + 4\sqrt{\epsilon} \tag{31}$$

---

**Theorem A.9** (Cluster-based Regret Bound is stronger than the General Bound). *If the following two assumptions hold:*

1.  $\sum_{k=1}^K w_T^k \gamma_S^k(f) \leq \sum_{k=1}^K w_S^k \gamma_S^k(f)$ .
2.  $X_S^k$  and  $X_T^k$  have Gaussian distributions for  $k = 1 \dots K$ .

Then we have

$$\sum_{k=1}^K w_T^k (\gamma^k)^* \leq \gamma^*. \quad (32)$$

Further, let

$$\epsilon_c(f) \doteq \sum_{k=1}^K w_T^k \gamma_S^k(f, g_S) + \sum_{k=1}^K w_T^k W_1(P_S^k, P_T^k) + \sum_{k=1}^K w_T^k (\gamma^k)^*$$

denote the sub-domain-based generalization bound, let

$$\epsilon_g(f) \doteq \gamma_S(f, g_S) + W_1(P_S, P_T) + \gamma^*$$

denote the general generalization bound without any sub-domain information. Then we have for all  $f$ ,

$$\epsilon_c(f) \leq \epsilon_g(f) + \delta_c \quad (33)$$

*Proof.* We will prove that  $\sum_{k=1}^K w_T^k (\gamma^k)^* \leq \gamma^*$ , where  $\gamma^* = \min_{f \in \mathbb{H}} \gamma_S(f, g_S) + \gamma_T(f, g_T)$ ,  $(\gamma^k)^* = \min_{f \in \mathbb{H}} \gamma_S^k(f, g_S) + \gamma_T^k(f, g_T)$

We have:

$$\begin{aligned} \gamma^* &= \min_{f \in \mathbb{H}} (\gamma_S(f, g_S) + \gamma_T(f, g_T)) \\ &= \min_{f \in \mathbb{H}} \left( \sum_{k=1}^K w_S^k \gamma_S^k(f, g_S) + \sum_{k=1}^K w_T^k \gamma_T^k(f, g_T) \right) \\ &= \min_{f \in \mathbb{H}} \left( \sum_{k=1}^K w_T^k \gamma_S^k(f, g_S) + \sum_{k=1}^K w_T^k \gamma_T^k(f, g_T) + \sum_{k=1}^K w_S^k \gamma_S^k(f, g_S) - \sum_{k=1}^K w_T^k \gamma_S^k(f, g_S) \right) \\ &= \min_{f \in \mathbb{H}} \left( \sum_{k=1}^K w_T^k (\gamma_S^k(f, g_S) + \gamma_T^k(f, g_T)) + \sum_{k=1}^K (w_S^k - w_T^k) \gamma_S^k(f, g_S) \right) \\ &\geq \min_{f \in \mathbb{H}} \left( \sum_{k=1}^K w_T^k (\gamma_S^k(f, g_S) + \gamma_T^k(f, g_T)) \right) \\ &\geq \sum_{k=1}^K \min_{f \in \mathbb{H}} (w_T^k (\gamma_S^k(f, g_S) + \gamma_T^k(f, g_T))) \\ &= \sum_{k=1}^K w_T^k (\gamma^k)^* \end{aligned} \quad (34)$$

where  $(\gamma^k)^* = \min_{f \in \mathbb{H}} \gamma_S^k(f, g_S) + \gamma_T^k(f, g_T)$

The fifth step is based on the assumption that  $\sum_{k=1}^K w_T^k \gamma_S^k(f) \leq \sum_{k=1}^K w_S^k \gamma_S^k(f)$ . The sixth step is based on  $\min\{f(x) + g(x)\} \geq \min\{f(x)\} + \min\{g(x)\}$

## B. Algorithm

Our framework is outlined in pseudo-code in Algorithm 1.



---

**Algorithm 1** Domain Adaptation via Rebalanced Sub-domain Alignment(DARSA)

---

**Input:** Source data  $X_S$ ; Source label  $y_S$ , Target data  $X_T$ ; coefficient  $\lambda_Y, \lambda_D, \lambda_c, \lambda_a$ ; learning rate  $\alpha$ ;  
Pretrain feature extractor and classifier with  $X_S$  and  $y_S$ , initialize  $\theta_E^S, \theta_E^T$ , and  $\theta_Y$  with pretrained weights. Initialize  $w_T^k$  and  $w_T^k$  with  $1/K$  for  $k = 1, 2, \dots, K$   
**repeat**  
    Sample minibatch from  $X_S$  and  $X_T$   
     $\theta_Y \rightarrow \theta_Y - \alpha \nabla_{\theta_Y} (\lambda_Y \mathcal{L}_Y + \lambda_D \mathcal{L}_D + \lambda_c \mathcal{L}_{intra} + \lambda_a \mathcal{L}_{inter})$   
     $\theta_E^S \rightarrow \theta_E^S - \alpha \nabla_{\theta_E^S} (\lambda_Y \mathcal{L}_Y + \lambda_D \mathcal{L}_D + \lambda_c \mathcal{L}_{intra} + \lambda_a \mathcal{L}_{inter})$   
     $\theta_E^T \rightarrow \theta_E^T - \alpha \nabla_{\theta_E^T} (\lambda_D \mathcal{L}_D + \lambda_c \mathcal{L}_{intra} + \lambda_a \mathcal{L}_{inter})$   
**until**  $\theta_E^S, \theta_E^T$ , and  $\theta_Y$  converge

---

## C. Details of Experimental Setup: Digit Datasets with Shifted Class Distribution

### C.1. Details of the Digit Datasets with Shifted Class Distribution

**MNIST  $\rightarrow$  MNIST-M:** For source dataset, we randomly sample 36000 images from MNIST training set with odd digits three times the even digits. For target dataset, we randomly sample 6000 images from MNIST-M constructed from MNIST testing set, with even digits three times the odd digits. To create MNIST-M dataset, we follow the procedure outlined in (Ganin et al., 2016) to blend digits from the MNIST over patches randomly extracted from color photos in the BSDS500 dataset. (Arbelaez et al., 2010).

**MNIST-M  $\rightarrow$  MNIST:** For source dataset, we randomly sample 36000 images from MNIST-M constructed from MNIST training set, with even digits three times the odd digits. For target dataset, we randomly sample 5800 images from MNIST testing set, with odd digits three times the even digits.

**USPS  $\rightarrow$  MNIST:** For source dataset, we randomly sample 3600 images from USPS training set, with even digits three times the odd digits. For target dataset, we randomly sample 5800 images from MNIST testing set, with odd digits three times the even digits.

**SVHN  $\rightarrow$  MNIST:** For source dataset, we randomly sample 30000 images from SVHN training set, with even digits three times the odd digits. For target dataset, we randomly sample 5800 images from MNIST testing set, with odd digits three times the even digits.

### C.2. Additional Empirical Analysis of our Proposed Generalization Bound

In our empirical analysis of our proposed generalization bound, we evaluate the bound on three additional task: 1) MNIST-M to MNIST, 2) USPS to MNIST and 3) SVHN to MNIST. All experiments are performed on our customized digit datasets with shifted class distribution (described in C.1). As shown in Figure 6, our empirical results demonstrate that our theory, i.e., Theorem 4.6 provides a stronger generalization bound than Theorem 4.1.

### C.3. Model Structures

For feature extractor, we employ a network structure similar to LeNet-5 (LeCun et al., 1998), but with minor modifications: the first convolutional layer produces 10 feature maps, the second convolutional layer produces 20 feature maps, and we use ReLU as an activation function for the hidden layer. Our feature space has 128 dimensions. For benchmarks, we utilize the network structures provided in the benchmark source code. In cases where experiments are not included in the source code, we use the same network architecture as our model to ensure fair comparisons. For classifier, we use a network structure with three fully connected layers with ReLU activation and a dropout layer with a rate of 0.5. Further details of each experiment can be found in our code.

### C.4. Model hyperparameters

We use Adaptive Experimentation (Ax) platform (Bakshy et al.; Letham et al., 2019), an automatic tuning approaches to select hyperparameters to maximize the performance of our method. We use Bayesian optimization supported by Ax with 20 iterations to decide the hyperparameter choice. We note that most of the SOTA comparisons are not specifically designed

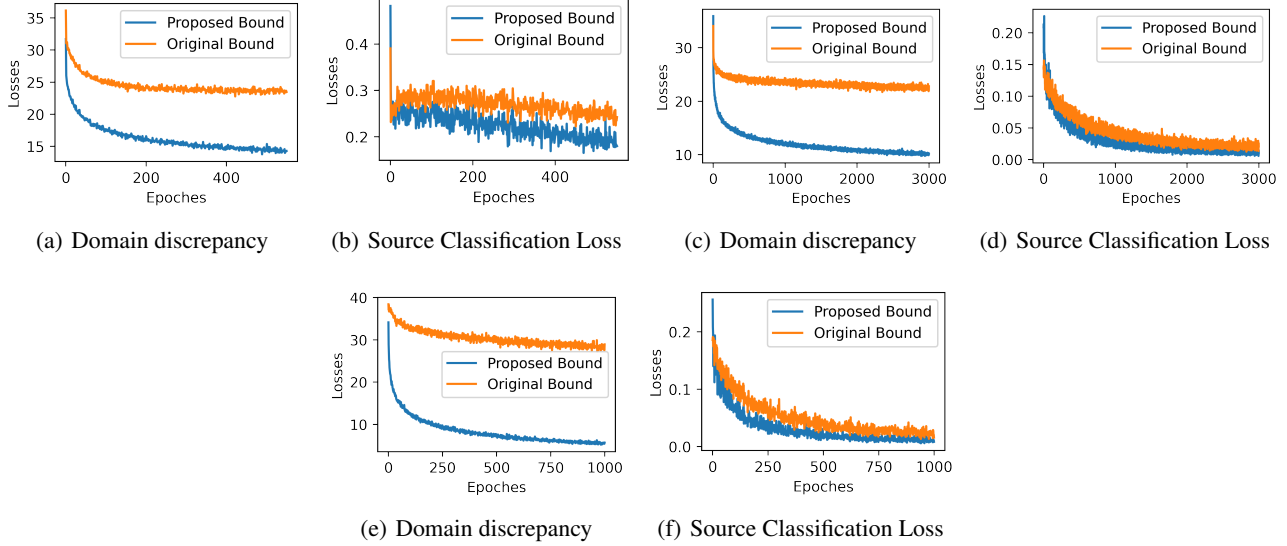


Figure 6. For tasks with shifted class distribution (1) we compare the domain discrepancy term ( $\mathcal{L}_D$ ) in our proposed bound to that in Remark 4.3, (2) Compare the source classification term ( $\mathcal{L}_Y$ ) in our proposed bound to that in 4.1. Task results shown in each subfigure: (a)(b) MNIST-M to MNIST, (c)(d) USPS to MNIST, (e)(f) SVHN to MNIST. All experiments are performed on our customized digit datasets with shifted class distribution (as described in C.1)

for shifted class distribution scenarios, and this setting caused issues in several competing. We used Ax to maximize their performance in domain shifting scenarios. Detailed model hyperparameters used for the class distribution shifting digits datasets are provided in Table 3.

## D. Details of Experimental Setup: TST Dataset with class distribution shifting

### D.1. Details of the TST Dataset with Shifted Class Distribution

The Tail Suspension Test (TST) dataset (Gallagher et al., 2017) consists of 26 mice recorded from two genetic backgrounds, Clock- $\Delta 19$  and wildtype. Clock- $\Delta 19$  is a genotype which has been proposed as a model of bipolar disorder while wildtype is considered as a typical or common genotype. Local field potentials (LFPs) are recorded from 11 brain regions and segmented into 1 second windows. For each window, power spectral density, coherence, and granger causality features are derived. Each mouse is placed through 3 behavioral contexts while collecting LFP recordings: home cage, open field, and tail-suspension. Mice spent 5 minutes in the home cage which is considered a baseline or low level of distress behavioral context. Mice spent 5 minutes in the open field context which is considered a moderate level of distress. Mice then spent 10 minutes in the tail suspension test which is a high distress context. Detailed model hyperparameters used for the class distribution shifting TST datasets are provided in Table 4.

### D.2. Model Structures

For feature extractor of the wildtype to bipolar task we use a network structure consisting of: a fully connected layer that maps our data to a feature space of 256 dimensions, with a LeakyReLU activation function; a fully connected layer that maps the feature space to 128 dimensions, and a Softplus activation function. For the bipolar to wildtype task, we use a network structure that includes: a fully connected layer that maps our data to a feature space of 256 dimensions, with a ReLU activation function; a fully connected layer that maps the feature space to 128 dimensions, with another ReLU activation function. For the classifier, we use a network structure that includes: three fully connected layers with ReLU activation and a dropout layer with a rate of 0.5. For benchmarks, we use the same network structures as our model to ensure fair comparisons, with the exception of DSN which has two fully connected layers with ReLU activation. Additional details on each experiment can be found in our code.

	MNIST to MNIST-M	MNIST-M to MNIST	USPS to MNIST	SVHN to MNIST
DARSA	batch size = 512, $\alpha = 0.01$ , $\lambda_Y = 0.4$ , $\lambda_D = 0.35$ , $\lambda_c = 1$ , $\lambda_a = 0.9$ , m = 30 SGD, momentum = 0.5	batch size = 512, $\alpha = 0.01$ , $\lambda_Y = 1$ , $\lambda_D = 0.5$ , $\lambda_c = 1$ , $\lambda_a = 1$ , m = 30 SGD, momentum = 0.4	batch size = 256, $\alpha = 0.01$ , $\lambda_Y = 1$ , $\lambda_D = 0.5$ , $\lambda_c = 1$ , $\lambda_a = 1$ , m = 30 SGD, momentum = 0.4	batch size = 256, $\alpha = 0.05$ , $\lambda_Y = 0.95$ , $\lambda_D = 0.11$ , $\lambda_c = 0.3$ , $\lambda_a = 0.11$ , m = 50 SGD, momentum = 0.4
DANN	batch size = 32 Adam, learning rate = 1e-4	batch size = 32 Adam, learning rate = 1e-5	batch size = 32 Adam, learning rate = 1e-4	batch size = 64 Adam, learning rate = 1e-4
WDGRL	batch size = 32 Adam, learning rate = 1e-5, $\gamma = 10$ , critic training step: 1, feature extractor and discriminator training step: 3	batch size = 64 Adam, learning rate = 1e-4, $\gamma = 10$ , critic training step: 5, feature extractor and discriminator training step: 10	batch size = 32 Adam, learning rate = 1e-4, $\gamma = 10$ , critic training step: 1, feature extractor and discriminator training step: 2	batch size = 32 Adam, learning rate = 1e-5, $\gamma = 10$ , critic training step: 1, feature extractor and discriminator training step: 3
DSN	batch size = 32 SGD, momentum = 0.8, learning rate = 1e-2, $\alpha = 0.01$ , $\beta = 0.075$ , $\gamma = 0.25$	batch size = 32 SGD, momentum = 0.8, learning rate = 0.01, $\alpha = 0.01$ , $\beta = 0.075$ , $\gamma = 0.25$	batch size = 32 SGD, momentum = 0.8, learning rate = 0.01, $\alpha = 0.01$ , $\beta = 0.075$ , $\gamma = 0.4$	batch size = 512 SGD, momentum = 0.5, learning rate = 1e-5, $\alpha = 0.46$ , $\beta = 0.61$ , $\gamma = 0.92$
ADDA	batch size = 64 Adam, learning rate = 1e-3, critic training step: 1, target model training step: 10	batch size = 64 Adam, learning rate = 1e-5, critic training step: 1, target model training step: 1	batch size = 64 Adam, learning rate = 1e-3, critic training step: 1, target model training step: 1	batch size = 64 Adam, learning rate = 1e-3, critic training step: 3, target model training step: 2
CAT	batch size = 512 SGD, learning rate = $\frac{0.01}{(1+10p)^{0.75}}$ , momentum = 0.9, p = 0.9, m = 30	batch size = 128 SGD, learning rate = $\frac{0.01}{(1+10p)^{0.75}}$ , momentum = 0.9, p = 0.9, m = 30	batch size = 128 SGD, learning rate = $\frac{0.01}{(1+10p)^{0.75}}$ , momentum = 0.9, p = 0.9, m = 30	batch size = 256 SGD, learning rate = $\frac{0.01}{(1+10p)^{0.75}}$ , momentum = 0.9, p = 0.9, m = 30
CDAN	batch size = 64 SGD, momentum = 0.9, learning rate = 0.01	batch size = 64 SGD, momentum = 0.9, learning rate = 0.01	batch size = 64 SGD, momentum = 0.9, learning rate = 0.01	batch size = 64 SGD, momentum = 0.9, learning rate = 0.1
pixelDA	batch size = 64 Adam learning rate = 0.0002, dim of the noise input: 10	batch size = 64 Adam learning rate = 0.0002, dim of the noise input: 10	batch size = 32 Adam, learning rate = 0.0001, dim of the noise input: 20	batch size = 32 Adam, learning rate = 0.0001, dim of the noise input: 20
DRANet	batch size = 32 Adam	batch size = 32 Adam	batch size = 32 Adam	batch size = 32 Adam

Table 3. Model hyperparameters used for digits datasets with class distribution shifting

### D.3. Model hyperparameters

Again, we use Adaptive Experimentation (Ax) platform (Bakshy et al.; Letham et al., 2019), an automatic tuning approaches to select hyperparameters to maximize the performance of our method. We use Bayesian optimization supported by Ax with 20 iterations to decide the hyperparameter choice. We note that most of the SOTA comparisons are not specifically designed

	Bipolar to Wildtype	Wildtype to Wildtype
DARSA	batch size = 128, $\alpha=1e-4$ , $\lambda_Y = 1$ , $\lambda_D = 0.4$ , $\lambda_c = 0.1$ , $\lambda_a = 0.9$ , $m = 50$ SGD, momentum = 0.6	batch size = 128, $\alpha = 0.001$ , $\lambda_Y = 0.7$ , $\lambda_D = 0.1$ , $\lambda_c = 0.1$ , $\lambda_a = 1$ , $m = 50$ SGD, momentum = 0.3
DANN	batch size = 32 Adam, learning rate = 1e-4	batch size = 32 Adam, learning rate = 1e-4
WDGRL	batch size = 32 Adam, learning rate = 1e-4, $\gamma = 10$ , critic training step: 1, feature extractor and discriminator training step: 2	batch size = 32 Adam, learning rate = 1e-5, $\gamma = 10$ , critic training step: 1, feature extractor and discriminator training step: 3
DSN	batch size = 64 SGD, momentum = 0.5, learning rate = 0.1, $\alpha = 1$ , $\beta = 1, \gamma = 1$	batch size = 32 SGD, momentum = 0.5, learning rate = 0.1, $\alpha = 1$ , $\beta = 1, \gamma = 1$
CAT	batch size = 128 SGD, learning rate = $\frac{0.01}{(1+10p)^{0.75}}$ , momentum = 0.9, $p = 0.9$ , $m = 3$	batch size = 128 SGD, learning rate = $\frac{0.01}{(1+10p)^{0.75}}$ , momentum = 0.9, $p = 0.9$ , $m = 3$
CDAN	batch size = 64 SGD, momentum = 0.9, learning rate = 0.1	batch size = 64 SGD, momentum = 0.9, learning rate = 0.1

Table 4. Model hyperparameters used for the class distribution shifting TST datasets

for shifted class distribution scenarios, and this setting caused issues in several competing. We used Ax to maximize their performance in domain shifting scenarios. Detailed model hyperparameters used for the class distribution shifting digits datasets are provided in Table 3.

## E. Accessibility of the Datasets

The MNIST, BSDS500, USPS, and SVHN datasets are publicly available with an open-access license. The Tail Suspension Test (TST) dataset (Gallagher et al., 2017) is available by request from the authors of (Gallagher et al., 2017).